Analyzing the Resiliency of XENONnT Background Models REU Program at Columbia University - Nevis Labs

Taylor Brown¹

¹Embry-Riddle Aeronautical University, Prescott

August 3, 2024

6 Abstract

5

10

11

12

13

XENONnT is a direct detection experiment in search of one viable dark matter (DM) candidate: weakly interacting massive particles (WIMPs). With its dual-phase Time Projection Chamber (TPC), XENONnT investigates incident particle interactions with xenon atoms in a rare signal search for theorized WIMP collisions. Due to the high rate of background events and the elusivity of the target signals, thorough background reduction is critical for DM direct detection experiments. This study investigates the resiliency and sensitivities of current XENONnT data analysis techniques and discusses the subsequent implications.



14 Contents

15	1	Introduction	3	
16 17 18 19	2	Modeling the Detector Response for ER Events in Liquid Xenon2.1 ER Emission Event Model	6	
20 21 22	3	ER Simulation and Model Parameters 3.1 Simulation Specifics and Workflow		
23 24 25 26	4	Mis-modeling Thresholds and Impacts4.1 Adding Imposter ER Events to Sampled Data Sets4.2 Goodness of Fit Evaluations	11	
27	5	Results and Discussion		
28	6	Acknowledgements	14	

29 1 Introduction

In 1933, California Institute of Technology's Fritz Zwicky found the high velocities of galaxies to be inconsistent with their observed masses; implying the existence of some elusive form of matter evading direct observation. [1] Due to its lack of interaction with the electromagnetic force, this missing matter was dubbed "dark matter" (DM), and remains the primary target of physics experiments around the world. A variety of candidates have been proposed and subsequently ruled out, but WIMPs remain a key player in question. WIMPs emerged naturally, independent of dark matter searches, in physics beyond the standard model making them well-motivated DM candidates. [7]

XENONnT aims to directly detect particle dark matter using a dual-phase Time Projection Chamber (TPC) filled with liquid xenon (LXe). LXe is a desirable detector medium with external radiation shielding capabilities due to its high atomic mass number and density. And since noble gasses have low rates of chemical interaction, they can be highly purified to reduce background. [5] Incident particles will interact with xenon atoms either electronically (by hitting a xenon atom's shell electron) or nuclearly (by hitting the atom's nucleus directly). Both interactions produce a pair of scintillation and charge signals that can be used to infer fundamental qualities of the incident particle. XENONnT's DM direct detection search works under the assumption that WIMPs scatter elastically off xenon atoms and produce nuclear recoils (NR), from which the resulting deposited energy can be measured. [2]

WIMP interactions are expected to be extraordinarily rare, and likely only happen within the detector a few times a year. Meanwhile, a plethora of non-WIMP events are recorded by the XENONnT experiments at much higher rates of occurrence. Thus, thorough background reduction is critical in XENON's search for elusive DM signals. Proactive background reduction measures are taken throughout the experiment, such as hosting the XENONnT detector underground at the INFN Laboratori Nazionali del Gran Sasso (LNGS) laboratory, incorporating active veto systems to identify neutrons and muons, as well as selecting a quiet, inner fiducial volume for analysis.

The XENONnT background is dominated by electronic recoils (ER). These ER events must be properly modeled and fit to differentiate background from the target data. Current XENONnT data analysis uses a Bayesian Band Fit (BBF) to fit data to the expected models, better understand LXe microphysics, and quantify the uncertainties in the regions of events. The model for ER events accounts for the physics behind the particle interactions, the detector response, and the reconstruction and correction of the signals. The BBF framework imposes a Markov-Chain Monte Carlo (MCMC) to find a best fit for the data versus the model, and constrain fundamental parameters in the process.

This method has proven reliable in the context of particle physics, and with it XENONnT has placed some of the most restrictive limits on WIMP cross sections thus far (see Figure 1). But the resiliency of the BBF framework when outliers are introduced to the data had yet to be quantified, until this study sought to investigate the impacts of outlier events on XENONnT data analysis techniques. In this paper, we discuss the nature and implementation of the BBF framework for ER event data, test the model and fit responses to outlier events in the calibration data sets, and analyze the subsequent potential impacts.

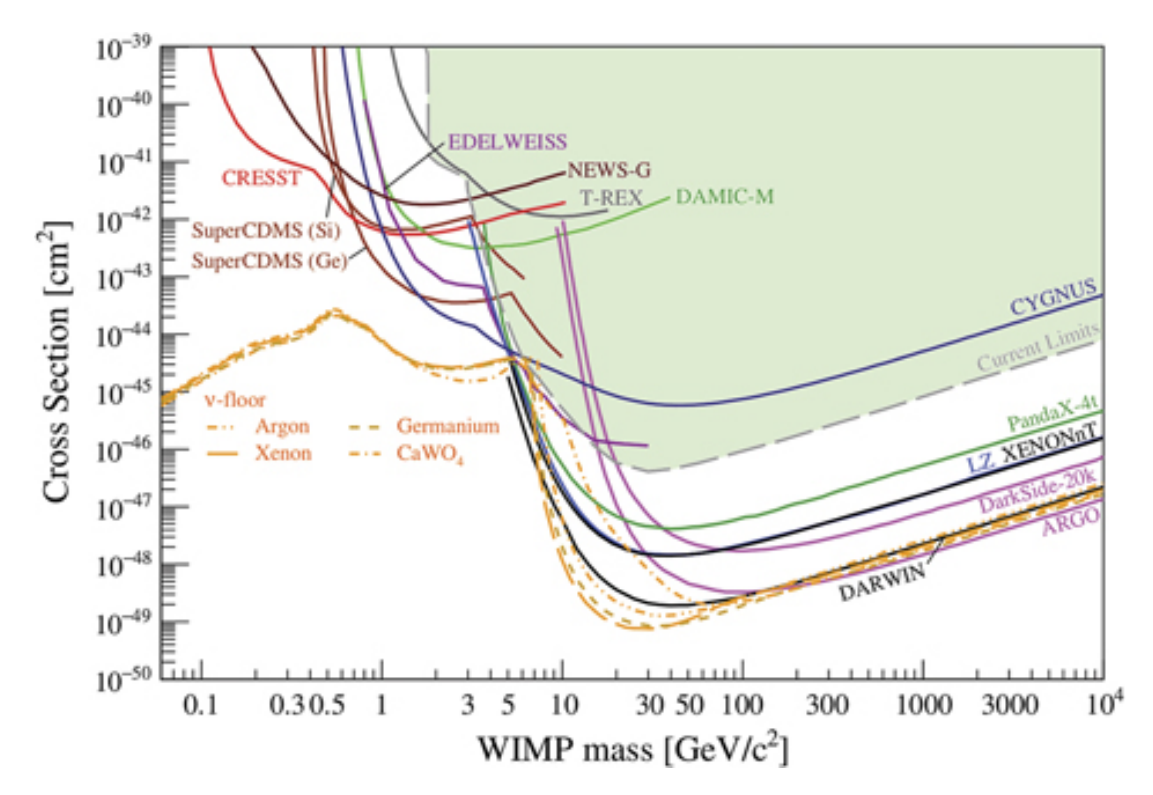


Figure 1: Sensitivities of current and predicted searches for spin-independent WIMP interactions. DARWIN is an anticipated dark matter detector that will be the product of multiple collaborations, including XENON.

2 Modeling the Detector Response for ER Events in Liquid Xenon

The majority of events in the XENONnT TPC fall into one of two categories: ER or NR. ER and NR events have different energy loss rates and thus dominate different regions of the S1-S2 space. (see Figure 2) Identifying these regions is critical, for they determine the interpretation of the science data. Due to the complexity of scattering in LXe, energy depositions within the detector must be analyzed by parameterization of the emission models. The XENONnT calibration and background reduction process use simulations created via informed signal response models that account for microphysics within the TPC, the detector response, and the reconstruction of event signals. These models are fit to calibration data from the regions of interest, and the parameters are constrained by a BBF.

It can be noted that the NR event model is similar to that of ERs, but is significantly more complicated and unpredictable due to energy loss and a higher recombination rate.

2.1 ER Emission Event Model

The ER emission model describes the production of scintillation photons and ionization electrons by the initial energy deposition. When incident particles scatter off of xenon electrons in the detector medium, the recoil energies excite and ionize the xenon atoms. The total number of detectable quanta, N_q , is the sum of the number of excitons N_{ex} and ions N_{ion} produced. [4] N_q is used to construct the

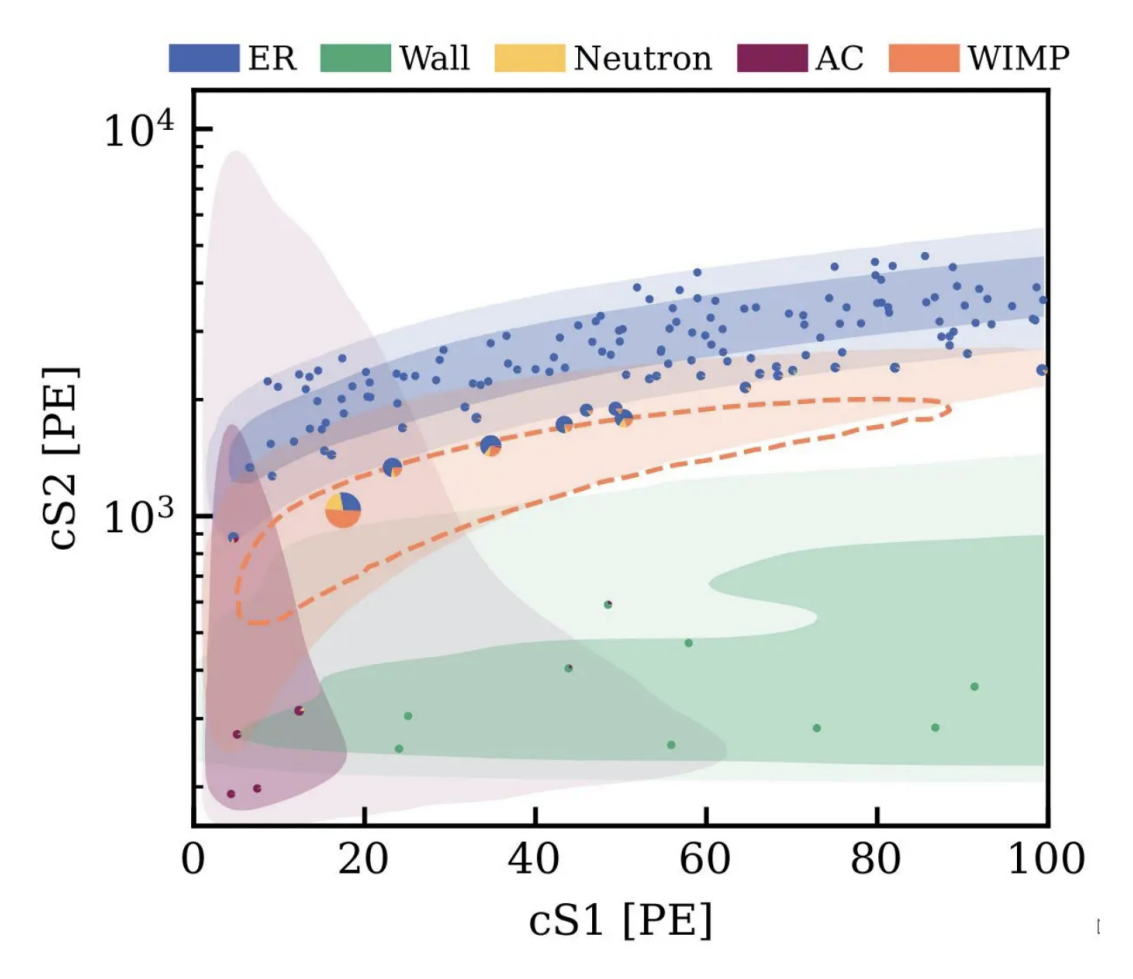


Figure 2: cS1 and cS2 space for XENONnT. WIMPs are expected to nuclearly recoil, while ER events dominate the background.

on intial deposited energy ϵ ,

$$N_q \sim Binom(\frac{\epsilon}{W}, L),$$
 (1)

where W is the average energy needed to creare an exciton or ion-electron pair in XENONnT, and the Linhard factor L describes the energy lost to heat (which is negligible for ER events).

A portion of the released electrons and ions will recombine and produce additional excitons. These electron-ion pairs are modeled by,

$$N_i \sim Binom(N_q, \frac{1}{1 + \langle N_{ex}/N_i \rangle}), \tag{2}$$

where $< N_{ex}/N_i >$ is the exciton-to-ion ratio, which is assumed to be constant for ER events in LXe. The subsequent ionization electrons may recombine with a xenon atom to form an excimer,

$$N_e \sim Binom(N_i, 1 - r), \tag{3}$$

where 1-r is the probability of recombination determined by r, the recombination factor. The recombination factor fluctuates, and follows a Gaussian distribution determined by the mean recombination fraction < r > and the recombination fluctuation Δr . The mean recombination fraction for

ER events $\langle r \rangle_{er}$ requires the deposited energy and electric field, and is described by a modified-Thomas-Imel (TI) box model. [8] Recombination results in the release of a scintillation photon N_{γ} when de-excited,

$$N_{\gamma} = N_i - N_e + N_{ex}.\tag{4}$$

These N_{γ} photons are detected by the detector's PMTs as a flash of 178 nm scintillation light and recorded as S1 signals. The produced ionization electrons N_e that do not recombine are drifted upwards by an induced electric field and subsequently extracted into the gas phase by an increased electric field. These ionization electrons are recorded as S2 signals. ER events have a lower recombination probability than NR events, resulting in smaller S1-S2 ratios. This is key for ER-NR differentiation. [3]

2.2 ER Detector Reconstruction Model

The ER detector reconstruction model is responsible for determining signal spatial coordinates and modeling the related efficiencies. The x and y coordinates are determined by the location of the detected signal on the PMTs, and z is calculates by the electron drift time. The light collection efficiency ϵ_L and the gas gain G (the number of photoelectrons per electron extracted into the gas layer) are spatially dependent. These are related to the energy scale parameters g_1' and g_2' , and modeled by

$$g_1'(x, y, z) = (1 + p_{dpe}) * \epsilon_L(x, y, z) * \epsilon_{QE} * \epsilon_{CE},$$

$$(5)$$

$$g_2'(x,y) = \epsilon_{ext}G(x,y), \tag{6}$$

where p_{dpe} is the probability of seeing an extra photoelectron emitted from the PMT cathode, ϵ_{ext} is the extraction efficiency, ϵ_{QE} is the quantum efficiency of the PMTs and ϵ_{CE} is the PMT's average collection efficiency.

The detector reconstruction model also considers inherent detector effects, software Reconstruction biases, and the resulting impacts on the event signals. For drifted electrons, electric field effects along the TPC walls and electron extraction efficiency impact the received S2 signals. The position coordinates are corrected using the photoelectrons from the PMT photocathode, the total proportional scintillation light detected, and the biases and fluctuations that occur within the detector. The final, corrected event signals, cS1 and cS2, are given by

$$cS1 = S1 \frac{g_1}{g_1'(x_r, y_r, z_r)},\tag{7}$$

$$cS2 = S2 \frac{g_2}{g_2'(x_r, y_r)} e^{\frac{z}{(\tau_e' * \nu_d)}}, \tag{8}$$

where x_r , y_r , and z_r are the corrected position coordinates. τ'_e represents the measured electron lifetime and ν_d is the electron drift velocity. From here, data quality is ensured by the data selection process, which is detailed in (?).

2.3 Fit to Calibration Data

The emission and reconstruction models are used to simulate the ER band and create a sample data set of 2000 events. This data set is fit to calibration data from the region of interest to constrain ER parameters and determine where it lies in the S1-S2 space. ER calibrations are performed using 220 Rn. The 220 Rn decay chain includes 212 Pb, whose β -radiation produces a uniform, low-energy ER

spectrum. (?)

The modeled ER events are fit to the calibration data using a GPU-supported Markov chain Monte Carlo (MCMC) algorithm. The MCMC samples from the distributions of the posterior parameters, and over the course of several iterations, fits to the model parameters. The MCMC is generally run until the samples converge to the posterior parameter distributions. For more detailed reading on MCMC specifics, see [6].

3 ER Simulation and Model Parameters

The models, simulations, and fits are executed using Appletree: XENONnT's software framework for event modeling, reconstruction, and analysis. This project included an ER simulation using the emission and detector reconstruction models, from which sample, 'toy' data sets were created to represent a selection of ER event signals. Experimental alterations were made to individual model parameters to test their impacts on the resulting ER band. This section describes ER simulation details and workflow, the model parameters, and the impacts of altered select parameters.

3.1 Simulation Specifics and Workflow

The ER simulation and sampling is as follows. The ²²⁰Rn calibration data was sampled and placed in 2-dimensional equi-probable bins. The ER component is initialized alongside an additional component to account for accidental coincidences (AC). AC events are formed by incorrect pairing of S1 and S2 signals in the calibration data set. The posterior parameters are defined by the marginal posteriors from the XENONnT 2024 WIMP search. [9] The simulation creates 1e6 events to visualize the ER event model. The simulated events are plotted in a 2-dimensional histogram with cS1 on the x-axis, cS2 on the y-axis, and the efficiencies act as weights. Unlikely events are disposed of from the simulation set by comparing the cS1 signal to its associated efficiency value, leaving 551961 events remaining. A toy data set of 2000 is sampled from this remainder to represent a selection of ER events.

3.2 Testing Select Parameter Impacts

The ER model takes 18 parameters; 6 fixed, 5 of normal or uniform distributions, and 7 free. Some parameters could be better constrained by setting the posterior values to those of the marginal posteriors determined via the XENONnT WIMP search in 2024 (see Table 2). [9] Parameters not listed include the ER rate, the AC rate, and select cuts for S1 and S2 acceptances and associated thresholds. The free parameters are associated with the recombination process in the emission model, and greatly impact the ER band shape at large. To better understand the elusive and vague free parameters in the context of this project, select free parameter posterior values were individually adjusted and used to create new ER simulations and sample data sets. The results were plotted in 2-dimensional histograms.

Multiple free parameters were altered, used to create sample data sets, and plotted to inform the direction of the project. For the reader's reference, this process is documented below for one select free parameter: py2. It should be noted that in some XENON documentation, this parameter is referred to as " $\delta_e r$, as is seen in Table 2. This parameter comes from the recombination model embedded

Parameter	Prior	Marginal Posterior	Unit
W	13.7 ± 0.2	$13.7^{+0.2}_{-0.2}$	eV
f	0.059	0.059	-
$< N_{ex}/N_i >$	0.06 - 0.20	$0.13^{+0.04}_{-0.04}$	-
γ	free	$0.13^{+0.03}_{-0.02}$	-
δ	free	$-0.34^{+0.07}_{-0.07}$	-
ω	free	57^{+15}_{-12}	keV
q_0	free	$1.32^{+0.17}_{-0.20}$	keV
q_1	free	$0.47^{+0.07}_{-0.05}$	keV
q_2	free	$0.030^{+0.002}_{-0.002}$	-
q_3	free	$0.47^{+0.40}_{-0.31}$	keV

Table 1: Table of prior and marginal posterior distributions of parameters in the ER emission model. Determined via the XENONnT WIMP search 2024. [9]

within the emission model. Specifically, py2 is included in the calculation of the field-dependent TI-model parameter,

$$\zeta = \frac{1}{4} \frac{E}{W} \frac{1}{1 + \langle N_{ex}/N_i \rangle} \times py0 \exp(-E/py1) F^{py2}$$
(9)

which is included in the calculation of the mean recombination fraction,

$$\langle r \rangle = \frac{1}{e^{-(E-q_0)/q_1} + 1} \left(1 - \frac{\log(1+\zeta)}{\zeta}\right),$$
 (10)

which represents the mean value of the true recombination probability distribution r,

$$r \sim Norm(\langle r \rangle, \Delta r). \tag{11}$$

As py2 increases, ζ increases, and therefore the mean recombination fraction increases. If the recombination fraction is greater, then more exciton-ion pairs will recombine and result in higher rates of s2 signals. The py2 parameter was changed from -0.14 to -0.68 with a step size of 0.07 to create an altered ER band simulation to sample toy data sets from. These data sets were plotted on top of the original, accepted simulation of the ER band in Figure 3. As the py2 value decreases from -0.14 to -0.68, the resulting data set moves upwards in the S1-S2 space. As seen in Table 2, the accepted marginal posterior value for py2 is $-0.34^{+0.07}_{-0.07}$, and thus the sample data set matches the ER band simulation best in Figure 3b.

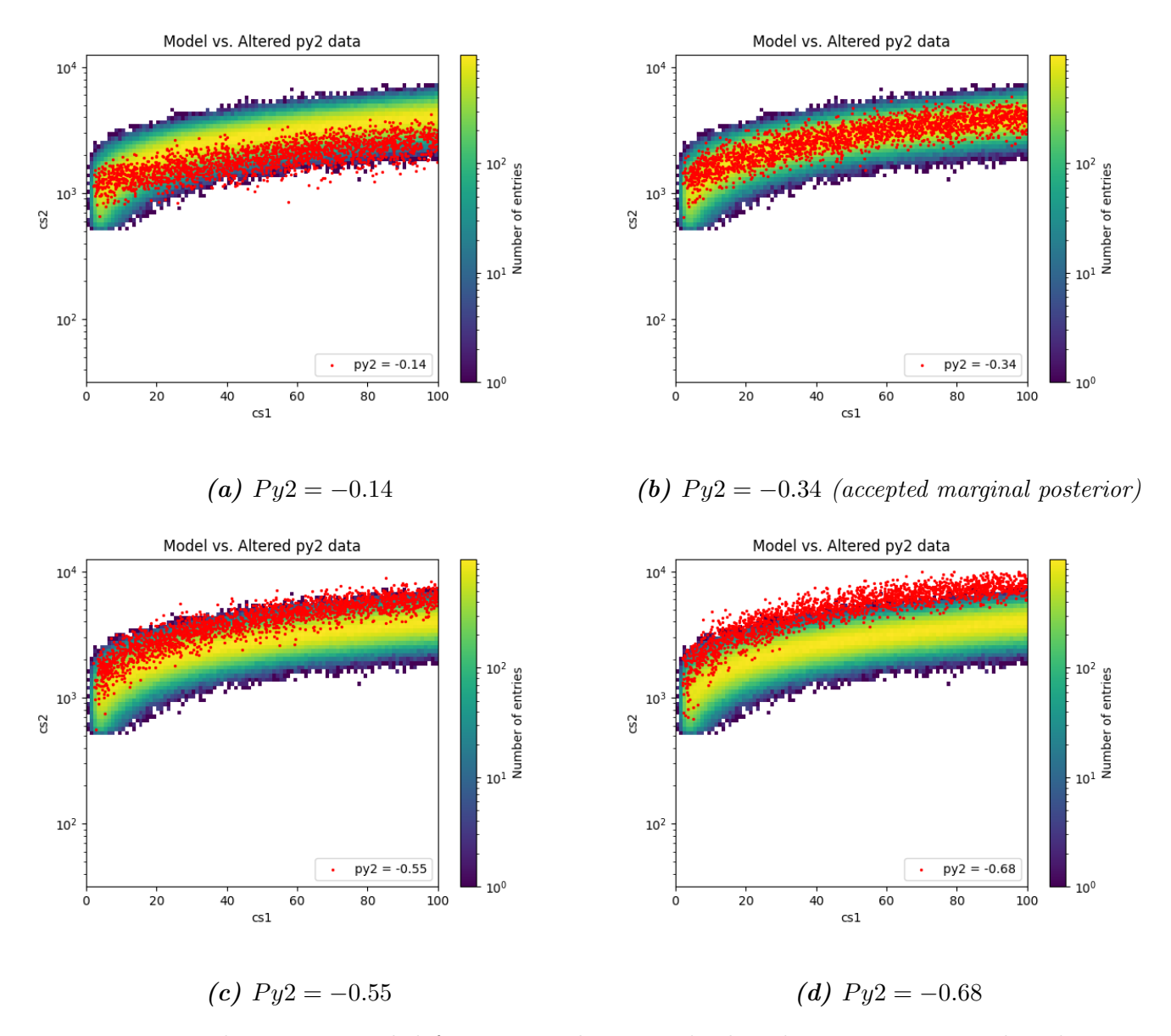


Figure 3: Toy data sets sampled from a simulation with altered py2 parameters plotted over ER band simulation without altered parameters.

4 Mis-modeling Thresholds and Impacts

The primary focus of this project was to study the resiliency of the ER model and fit when tested with outliers in the calibration data. The study is concerned with the thresholds of tolerance the models have for outliers in different regions as well as which goodness of fit tests were more capable of detecting the effects of outliers. This section describes the method of adding increasing quantities of outliers to the sample data sets and evaluating their goodness of fit prior to and after the MCMC.

4.1 Adding Imposter ER Events to Sampled Data Sets

The impacts of outlier events were tested in the regions of 2 to 3σ , upper 2 to 3σ , and lower 2 to 3σ deviations, as well as uniform distributions across the ER region of the S1-S2 space. The

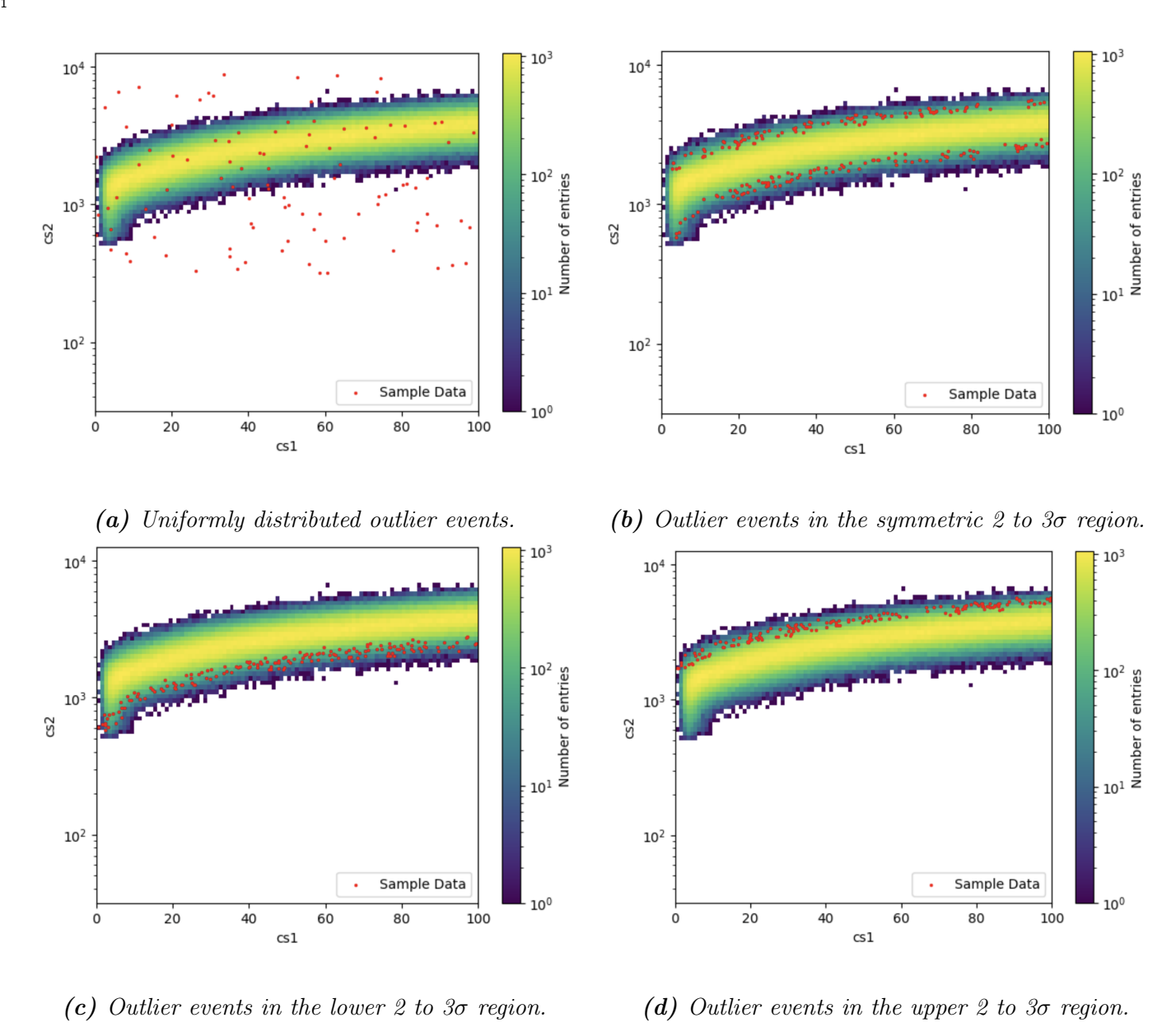


Figure 4: The distributions of outlier events that were selected for this study.

Note that uniformly distributed outlier events were restricted to the general ER region of the S1-S2 space for a more relevant study. Outliers in the median to 1σ region were initially considered, but largely abandoned in this study for events falling within a 1σ -deviation from the median are likely ER events, and not outliers. Outlier events were increasingly added with a set step size to 1 sample data set for each region. Maintaining the same sample data set for each set of increased values was critical to maintain consistency.

As of current standing, magnitude of outlier events existing in calibration data is unknown. Similarly, it is unknown where outlier events would most likely fall if they did exist in the collected calibration data sets. This project was not aimed at analyzing the calibration data directly, but instead looked to determine thresholds where XENONnT's current models and goodness of fit eval-

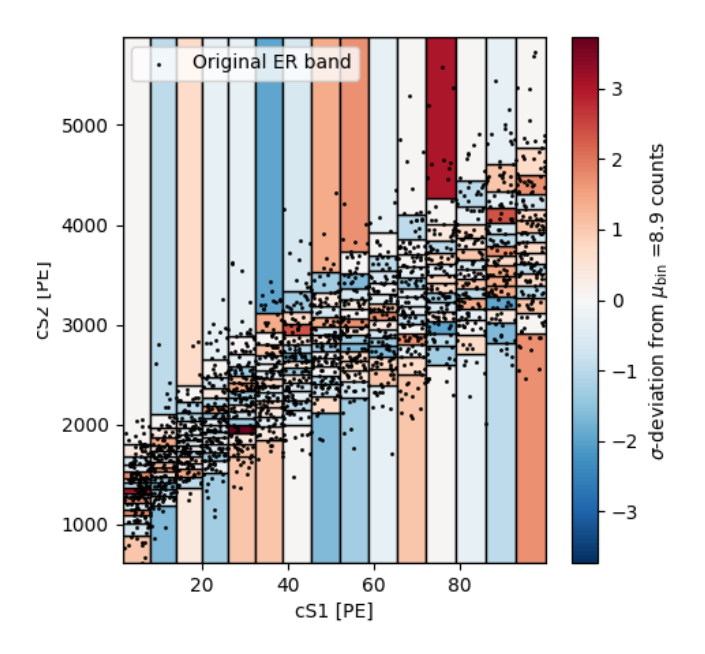


Figure 5: Example GOF evaluation on a toy data set.

uations will no longer tolerate outlier events in various regions of the S1-S2 space.

4.2 Goodness of Fit Evaluations

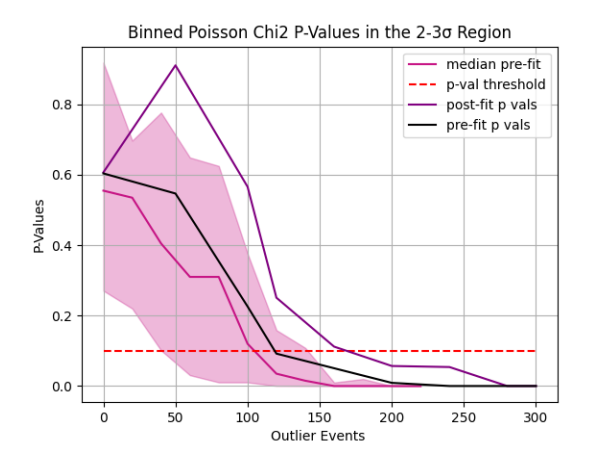
 To evaluate how well the ER models describe the calibration data when faced with imposter ER events, we calculated the probability (p) values of the data prior to and after the MCMC using our Goodness of Fit (GOF) evaluations. The GOF evaluation used for this study was a Binned Poisson χ^2 evaluation to determine the compatibility of the model and calibration data. A χ^2 for binned data with a Poisson distribution can be calculated via,

$$\chi^2 = \sum_{i=0}^{\infty} \frac{(N_i - \langle N_i \rangle)^2}{\langle N_i \rangle}$$
 (12)

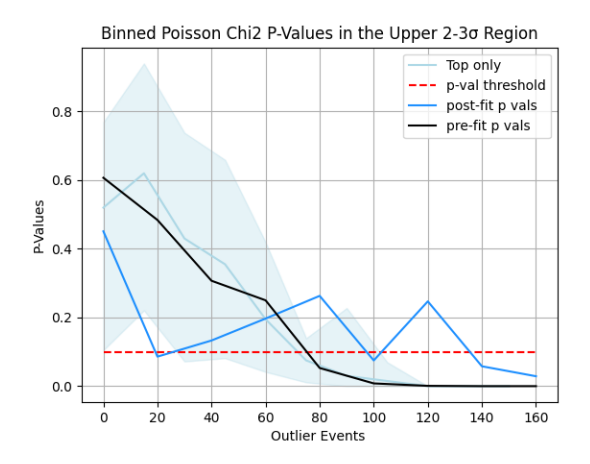
where *i* represents your number of counts in a specified period, N_i is the observed frequency, and $\langle N_i \rangle$ is the frequency predicted by the model. In Appletree, the Binned Poisson χ^2 test uses equiprobable binning to distribute the data and compare the observed number of counts to the expected number. An example GOF evaluation is depicted in Figure 5. The GOF evaluations provide an associated Probability (p) value that is our measure of how well the model describes the calibration data.

4.3 Determining Sensitivity Thresholds

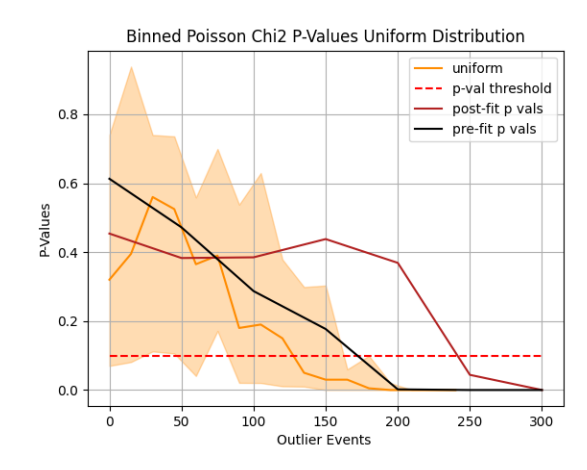
P-value calculations using the Binned Poisson χ^2 GOF evaluation were evaluated for the specified types of mis-modeling for increasing numbers of imposter ER events both prior to and after the MCMC.



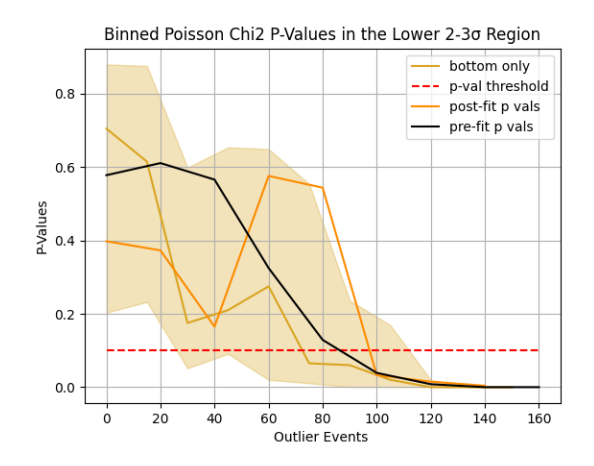
(a) P-value calculations for mis-modeling in the symmetric 2 to 3 σ range.



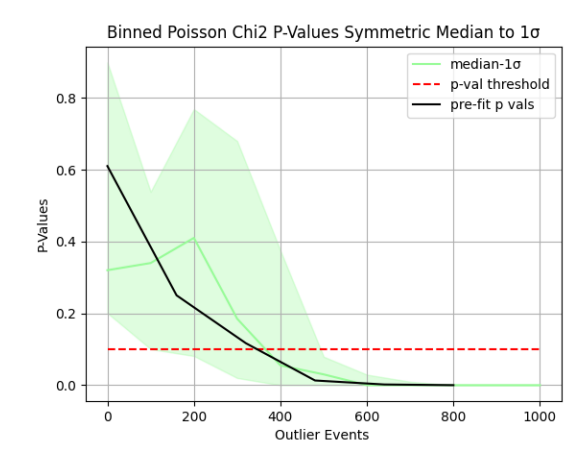
(c) P-value calculations for mis-modeling in the positive 2 to 3 σ range.



(b) P-value calculations for uniformly distributed mis-modeling.



(d) P-value calculations for mis-modeling in the negative 2 to 3 σ range.



(e) P-value calculations for mis-modeling in the median to 1 σ range.

Figure 6: The results of the sensitivity/threshold tests performed by this study for the specified types of mis-modeling.

For each type of mis-modeling, we calculated the p-values for 20 random data sets prior to the MCMC while steadily increasing the quantity of imposter ER events. Then, we sampled one random data set and performed the same p-value calculations with the same GOF evaluation (represented by the black lines in each of the Figure 6 subplots). Subsequently, we took that random data set and re-calculated the p-values after performing the MCMC. It was expected that the post-fit p-values would be higher than those calculated prior to the fit, as the MCMC is supposed to better constrain the model's description of the calibration data and thus increase the threshold at which the model, fit, and GOF evaluation will detect mis-modeling. For some tests, particularly the one for the -2 to -3σ range (Figure 6d), this was not explicitly the case. We believe this is due to potential noise in the sample data set stemming from the method of generating the outlier imposter ER events. From these tests, we were able to determine the general thresholds for when the model, MCMC, and associated GOF test are able to detect mis-modeling in specified regions (Table 2).

Mis-modeling Type	Threshold Prior-fit	Threshold Post-fit
$2 \text{ to } 3\sigma$	\sim 220 events (9.9%)	$\sim 280 \text{ events } (12.3\%)$
-2 to -3 σ	~ 140 events (6.5%)	-
$+2 ext{ to } +3\sigma$	\sim 120 events (5.6%)	$\sim 160-180$ events $(7.4-8.3\%)$
Uniform	~ 200 events (9%)	~ 300 events (13.6%)
Median to 1σ	\sim 700 events (26%)	-

Table 2: Quantity of imposter ER events needed for GOF evaluation to consistently provide a p-value of 0.

The post-fit test for mis-modeling in the -2 to -3 σ region was inconclusive, likely due to the aforementioned noise in the GOF evaluation as well as a likely issue with binning in this region of the ER band. Additionally, post-fit p-value calculations were not determined for the median to 1σ range due to time constraints.

5 Results and Discussion

It was found that the uniformly distributed mis-modeling and the mis-modeling in the symmetric 2 to 3 σ ranges required a higher quantity of imposter ER events to be detected than the asymmetric 2 to 3 σ ranges. This is likely due to the less concentrated nature of the mis-modeling. The more condensed the mis-modeling, the more likely it will be detected earlier by the GOF evaluation since the Binned Poisson χ^2 test does not register the distance of events from the median. Similarly, it is sensical that mis-modeling in the median to 1σ range would be more difficult to detect. Events that fall within this range are likely true ER events, and mis-modeling in this region is less of a concern. Thus, it follows that it would require a significant portion of the data set for the mis-modeling in this region to be detected. The thresholds for mis-modeling detection prior to and after the MCMC pose a variety of implications. It was found that Appletree is capable of fitting large deviations in the calibration data, which requires more critical analysis of the calibration data prior to fitting. This is not detrimental in itself, as Appletree's purpose is to constrain the model parameters to the calibration data. But this does increase the threshold for which mis-modeling becomes detectable,

and calls for skeptical analysis of the calibration data prior to the MCMC.

Ultimately, if any mis-modeling exists within ER analysis process, then the model will not accurately describe ER events. It is necessary that XENONnT is highly critical of the calibration data prior to and after the fit to mitigate the risk of mis-modeling impacting the statistical inference of the science data.

$_{^{279}}$ 6 Acknowledgements

273274

275

276

277

278

This material is based upon work supported by the National Science Foundation under Grant No. PHY-2349438. Additional thanks to Prof. Elena Aprile, the XENONnT Collaboration, Shenyang Shi, Knut Moraa, and the Nevis Laboratories community.

References

- Heinz Andernach and Fritz Zwicky. "English and Spanish Translation of Zwicky's (1933) The
 Redshift of Extragalactic Nebulae". In: arXiv e-prints, arXiv:1711.01693 (Nov. 2017), arXiv:1711.01693.

 DOI: 10.48550/arXiv.1711.01693. arXiv: 1711.01693 [astro-ph.IM] (cit. on p. 3).
- ²⁸⁷ [2] E. Aprile et al. "First Dark Matter Search with Nuclear Recoils from the XENONnT Experiment". In: 131.4, 041003 (July 2023), p. 041003. DOI: 10.1103/PhysRevLett.131.041003. arXiv: 2303.14729 [hep-ex] (cit. on p. 3).
- E. Aprile et al. "XENON1T dark matter data analysis: Signal and background models and statistical inference". In: 99.11, 112009 (June 2019), p. 112009. DOI: 10.1103/PhysRevD.99. 112009. arXiv: 1902.11297 [physics.ins-det] (cit. on p. 6).
- E. Aprile et al. "XENON1T dark matter data analysis: Signal reconstruction, calibration, and event selection". In: 100.5, 052014 (Sept. 2019), p. 052014. DOI: 10.1103/PhysRevD.100.052014. arXiv: 1906.04717 [physics.ins-det] (cit. on p. 4).
- Elena Aprile. "The XENON program for dark matter direct detection". In: *Nuclear Physics B* 1003, 116463 (June 2024), p. 116463. DOI: 10.1016/j.nuclphysb.2024.116463 (cit. on p. 3).
- Daniel Foreman-Mackey, David W. Hogg, Dustin Lang, and Jonathan Goodman. "emcee: The MCMC Hammer". In: 125.925 (Mar. 2013), p. 306. DOI: 10.1086/670067. arXiv: 1202.3665 [astro-ph.IM] (cit. on p. 7).
- Teresa Marrodán Undagoitia and Ludwig Rauch. "Dark matter direct-detection experiments". In: Journal of Physics G Nuclear Physics 43.1, 013001 (Jan. 2016), p. 013001. DOI: 10.1088/0954-3899/43/1/013001. arXiv: 1509.08767 [physics.ins-det] (cit. on p. 3).
- J. Thomas and D. A. Imel. "Recombination of electron-ion pairs in liquid argon and liquid xenon". In: 36.2 (July 1987), pp. 614–616. DOI: 10.1103/PhysRevA.36.614 (cit. on p. 6).
- 306 [9] XENON Collaboration et al. "XENONnT WIMP Search: Signal & Background Modeling and Statistical Inference". In: *arXiv e-prints*, arXiv:2406.13638 (June 2024), arXiv:2406.13638. DOI: 10.48550/arXiv.2406.13638. arXiv: 2406.13638 [physics.data-an] (cit. on pp. 7, 8).